ISSN: 0067-2904

Land Surface Temperature and Soil Moisture Index Assessments Using Satellite Imagery at Karbala City

Yusra K. H. Moussa
Remote Sensing & GIS Department, College of Science, University of Baghdad, Baghdad, Iraq

Received: 11/9/2024 Accepted: 26/ 3/2025 Published: 28/2/2026

Abstract

The use of remote sensing technology and modeling methodologies to monitor changes in land surface temperature (LST) and soil moisture index (SMI) has become an essential reference for making decisions on sustainable land use. This study aims to estimate LST and SMI in Karbala Province to contribute to land management, urban planning, or climate resilience in the region; as a result of environmental changes in recent years, LANDSAT Satellite Imagery from 2013-2023 was implemented to estimate the LST and SMI indexes. ArcGIS 10.7 package was used to calculate the indices, and the normalized mean vegetation index (NDVI) was calculated as it is closely related to extracting the LST and SMI indices. The results showed that extracting the vegetation index, atmospheric radiation, satellite brightness temperature, and land surface emissivity using Landsat-8 bands and processing them on ArcGIS facilitates the estimation of each LST and SMI index. The results showed a complete inverse correlation between LST and SMI; the correlation coefficient during 2013 and 2023 was -1 and -0.999, respectively.

Keywords: Landsat 8, ArcGIS, normalized difference vegetation index (NDVI), land surface temperature (LST), and soil moisture index (SMI).

تقييم درجة حرارة سطح الأرض ومؤشر رطوبة التربة باستخدام صور الأقمار الصناعية في مدينة كربلاء

يسرى كاظم حسون موسى
قسم التحسس النائي ونظم المعلومات الجغرافية , كلية العلوم, جامعة بغداد, بغداد, العراق

الخلاصة

أصبح استخدام تقنية الاستشعار عن بعد ومنهجيات النمذجة لرصد التغيرات في درجة حرارة سطح الأرض (LST) ومؤشر رطوبة التربة (SMI) مرجعًا أساسيًا لاتخاذ القرارات بشأن الاستخدام المستدام للأراضي وحساب التبخر والنتح السطحي. تم تنفيذ صور أقمار LANDSAT الصناعية من 2013–2023 لتقدير مؤشرات LST و SMI في محافظة كربلاء، واستخدام حزمة ArcGIS 10.7 لحساب المؤشرات، وتم حساب مؤشر الغطاء النباتي المتوسط (NDVI) باستخدام النطاقين 4 و 5، ثم LST و SMI. أظهرت النتائج أن استخراج مؤشر الغطاء النباتي والإشعاع الجوي ودرجة حرارة سطوع القمر الصناعي وانبعاث سطح الأرض باستخدام نطاقات Landsat-8 ومعالجتها على ArcGIS، يسهل تقدير كل من مؤشرات (LST) و

Email: yosra.k@sc.uobaghdad.edu.iq

(SMI)، وأظهرت النتائج وجود علاقة عكسية كاملة بين LST و SMI. وسجل معامل الارتباط خلال الأعوام 2013 و2023 قيم (−1) و(−0.999) على التوالي.

1. Introduction

Vegetation indices are commonly used to see how changes in green cover affect surface temperature (LST), which is an important parameter in exploring surface matter exchange and surface energy balance [1]. Plants can influence LST by selectively absorbing and reflecting solar radiation energy and regulating latent and sensible heat exchange [2]. The NDVI is an important index used to study the relationship between LST and vegetation [3] [4], which is a critical parameter in analyzing urban thermal patterns [5] and important for improving urban liveability [6]. Remote sensing is "the science and art of obtaining information about an object, area, or phenomenon by analyzing data obtained by a device that is not in contact with the object, area, or phenomenon under investigation" [7]. The emergence of the general term remote sensing and its association with geographic information systems (GIS) has been of great importance in the fields of meteorology, climatology, urban planning, and sustainable development [8] [9]. The reliance on scientific techniques has resulted in overcoming the difficulties researchers face in obtaining accurate data over long periods [10] [11]. Remote sensing has made its way very quickly due to the accuracy of obtaining information from aerial images (aircraft, aerial photographs, and satellites) [12], where it has been used mainly to solve many issues related to the earth and the atmosphere, whether at the local, or national, or global scale [13] [14]. Several studies have shown that the weather conditions of a specific city vary depending on its urban nature [15]. The use of remote sensing information has the advantage of obtaining a high-resolution coverage of the visible light spectrum reflectance on vegetation types. The study aims to evaluate the LST, LSM, and NDVI using the Landsat satellite images. [16]. Since this relationship is affected by many complex factors, it is necessary to continue exploring it [17]. It has become necessary to study LST with land use and its associated changes [18]. Given the close relationship between vegetation strength and available soil moisture, especially in arid and semi-arid regions, the normalized difference in vegetation index and satellite-derived land surface temperature has been used to assess drought conditions [19]. Therefore, remote sensing data from Landsat with a spatial resolution of 30×30 m were used to generate updated data to characterize vegetation patterns and thermal environments [20].

In general, Karbala has witnessed environmental changes in recent years. In 2017, Israa and Amjed studied the NDVI and the Green Normalized Difference Vegetation Index (GNDVI) and used techniques to detect the change in the studied area during the years 1985, 1995, 2005, and 2015; the results showed an increase in vegetation cover [21]. In 2022, Weam and Iman investigated climate data for rainfall and temperature for seventy years (1941-2009). The result was an apparent decrease in rainfall rates, making its climate continental and dry. The city of Karbala also suffers from a large water deficit of up to 93% [22]. Habeeb and others studied the hydrological analysis of the areas west of Karbala using field surveys and GIS technology [23]. Although previous studies have made great strides in the environmental field, the scientific techniques of remote sensing have broad horizons that enable us to determine surface temperature and soil moisture index indicators. The study aims to evaluate the LST, SMI, and NDVI using the Landsat satellite images, leading to sustainable land management or urban planning in Karbala.

Materials and Methods:

1. Study area:

Karbala Province is located in the Mesopotamian plain, 110 km southwest of Baghdad's capital, Iraq, about 36 m above sea level. The borders of the study area are occupied from the east and northeast by the Babylon governorate, from the west and northwest Anbar governorate, and the south Najaf governorate. It is located between the northern latitudes (31.75º) and (33.5º) and the eastern longitudes (43.2º) and (44.5º). It occupies an area estimated at 30 km^2 and is bordered by Babylon Province to the east and northeast, Anbar Province to the west and northwest, and Najaf Province to the south [24]. The study area is located in the southern part of the northern temperate zone, at the end of the eastern edge of the land area connected to the west with a desert climate, where the maximum temperature in the summer reaches 50 C^0. In contrast, the temperature drops to below $0C^0$ in the winter, and the surface terrain of the city includes some dunes, which these features impact the variability of LST, and some valleys and water bodies containing rainwater, which impact the variability of SMI [25].

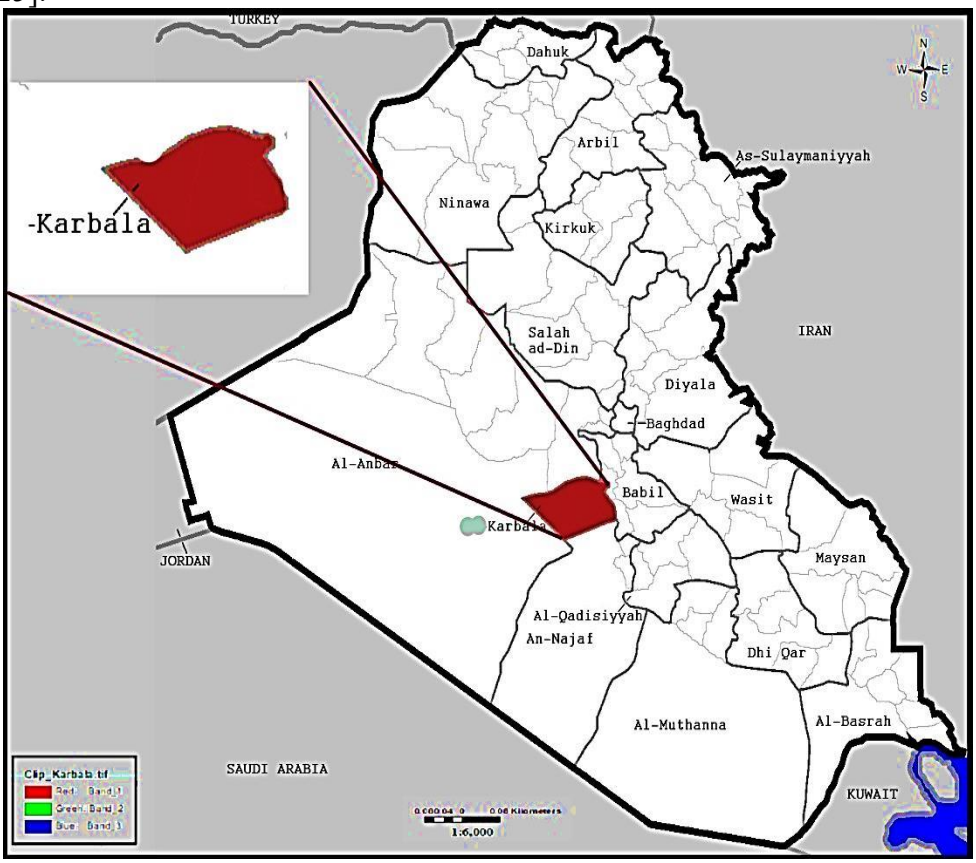

Figure 1: Study area

2. Data sets and methods:

The data used in this study include the United States Geological Survey (USGS, http://earthexplorer.usgs.gov) website that includes thermal infrared remote sensing data from Landsat 8 OLI/TIRS (band 10) [26], digital elevation model (DEM), and shapefile data for Karbala Province. Images were taken on September 3rd, 2013, and August 12th, 2023, the map's scale (1:500,000).

Landsat 8 has two scientific instruments: the Operational Land Imager (OLI) has bands 1-9 and is used to collect non-thermal data, which has a resolution of 30 m, and the Thermal Infrared Sensor (TIRS) has bands 10,11 and is used to collect thermal data, which has a

resolution of 100 m and were used to collect LST data that stray light effect is enough in Band 10, Band 11 to make the data useful across a wide array of applications [27]. Cloud-free data from 2013 to 2023 was selected to avoid cloud' effects in the study area's analysis. ArcMap 10.7 software was used to correct the data for atmospheric distortions and extract the boundaries of the study area. The corrected Landsat data was used to generate NDVI and LST maps, and the relationship between LST and NDVI was then investigated. Figure 2 shows a diagram of how to evaluate the surface temperature index and soil moisture.

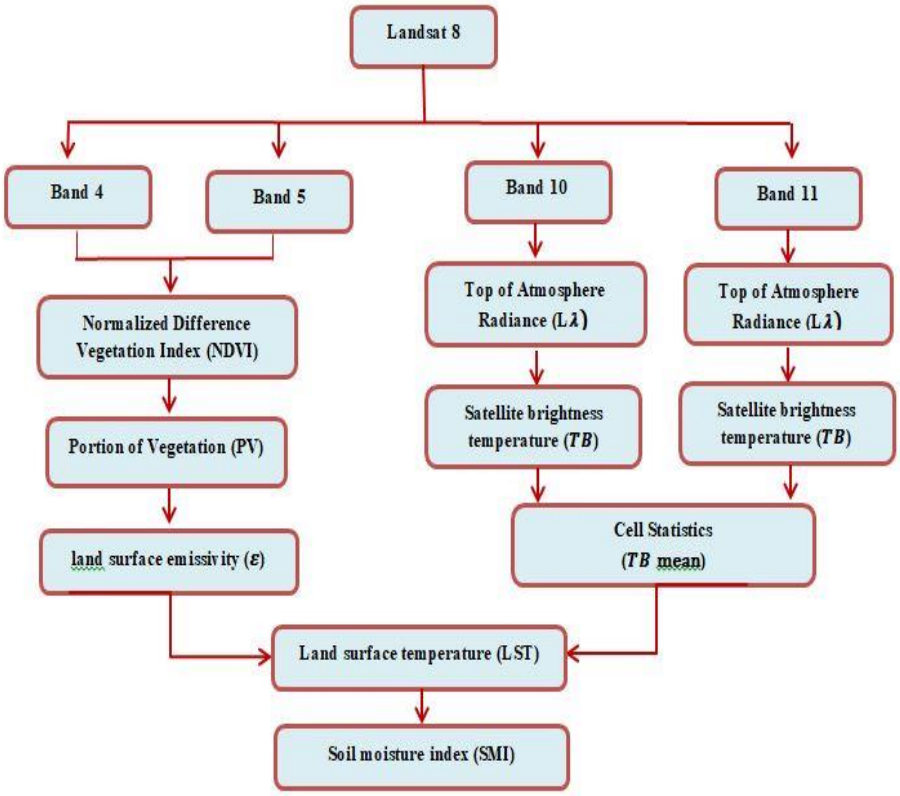

Figure 2: A diagram showing how to evaluate the surface temperature index and soil moisture

3. Satellite Imagery Acquisition:

ArcGIS v10.7 was employed in this study; satellite images were obtained from the USGS Earth Explorer database. Landsat 8 carries Operational Land Image (OLI)/TIRS sensors from Collection 2/ Level 1 with a ground resolution of 30 m from the sensor, Table 1.

Table 1: Information on the images of Landsat were used in the study

NO.	Launched Date	cloud cover	Path/Row	Satellite Image	Image level	Sensor Type	Source
1	12/08/2013	0.00	168/38	LANDSAT-8	Collection 2/ Level 1	Operational Land Image (OLI)/TIRS	USGS Earth Explorer Database
2	03/08/2013	0.00	169/38				
3	24/08/2013	0.08	169/37				
4	14/08/2023	0.00	169/38				
5	14/08/2023	0.00	169/37				
6	07/08/2023	0.00	168/38				

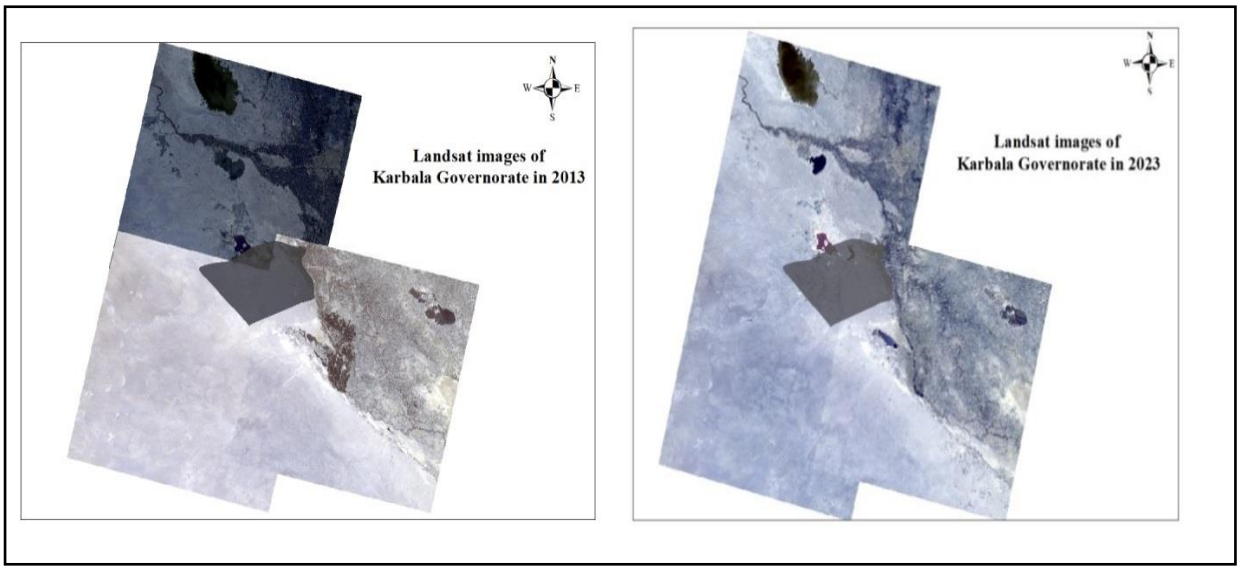

Figure 3: Landsat images of Karbala Province in 2013 and 2023

4. **Methodology:**

The Landsat 8 satellite image was obtained from the official USGS website, earthex plorer.usgs.gov. Bands (4 and 5) and thermal bands (10 and 11) were used and processed using ArcGIS 10.7. The following sections explain in detail the methods of processing land cover indices.

4.1. Upper atmosphere radiation (Lλ): The remote sensing instruments directly measure radiation. Radiation includes backscattered radiation from pixels and radiation reflected from the surface and clouds. The upper atmosphere radiation was calculated using thermal bands, which are bands (10) and (11) [28]. The TOA (Top of Atmosphere) spectral radiance is determined using the following equation:

$$\boldsymbol{L(\lambda) = (M_L \times Q_{cal}) + A_L} \quad \text{..... (1)}$$

Where:

• L(λ): Top of Atmosphere spectral irradiance was measured directly by remote sensors (includes radiation reflected from the surface, radiation bounced off neighboring pixels, and radiation reflected from clouds).

• ML: Radiance multiplicative band from the metadata (RADIANCE MULT BAND x, where x is the band number).

• Q(cal) = Quantized and Calibrated Standard Product pixel value (DN) for bands 10 and 11 (value taken from Metadata file)

• AL: Radiance adds bands 10 and 11 from the metadata (RADIANCE_ADD_BAND_x, where x is the band number).

4.2. Satellite brightness temperature (BT): It was calculated using the thermal ranges (10 and 11), and to convert the brightness temperature from Kelvin (k) to Celsius (C^0), the equation (2) was used: [29] [30]

$$\boldsymbol{BT = K2/ln\,(k1/L(\lambda) + 1) - 273.15} \quad \text{..... (2)}$$

Where:

- BT: Top of Atmosphere brightness temperature C^o
- K1, K2: constant for band x, where x is the band number.

4.3. Natural Vegetation Index Method for Correcting Emissivity:

The Normalized Difference Vegetation Index (NDVI) was calculated using Band 4, which corresponds to the red spectrum, which plants absorb, and Band 5, which corresponds to near-infrared (NIR), which represents radiation reflected from plants, Eq. (3), [31].

$$NDVI = (NIR - RED)/(NIR + RED) \quad \text{..... (3)}$$

Where:
NIR: is the digit number in the Near-Infrared band.
RED: is the digit number in the red band.

Table 2: Landsat band information

Source	Bands	Wavelength(μm)
Landsat8 (OLI)	4 (Red)	0.636-0.673
	5 (NIR)	0.851-0.879

The NDVI values range between ⁻1 and 1; dense vegetation refers to a more positive NDVI value, and the surface without vegetation has an NDVI value close to zero or decreases negatively. The law NDVI values generally refer to soil and other ground categories. The results will appear in grayscale whenever the color means white, the presence of dense vegetation cover. Whenever it becomes less and tends to darken, the plant lights up until it turns black, which means there is no vegetation in the area [32]. The amount of vegetation is crucial in determining the percentage of vegetation (Pv) directly linked to the NDVI. Additionally, the emissivity (must be calculated, as it is closely related to Pv). These parameters are essential for accurate surface characterization and thermal emission modeling in remote sensing applications:

4.4. Portion of Vegetation (Pv): It stands for vegetation ratio; it is calculated to the equation: [33]

$$Pv = ((NDVI - NDVImin)/(NDVImax - NDVImin))^2 \quad \text{.....(4)}$$

Where: NDVI max = (Maximum DN) from NDVI
NDVI min = (Minimum DN) from NDVI

4.5. Land surface emissivity(E): This represents a factor for predicting emitted radiation, the efficiency of transferring thermal energy through the surface to the atmosphere, and was calculated by calculating the percentage of vegetation cover (Pv) according to the equation: [34].

$$E = m \times PV + n \quad \text{..... (5)}$$

Where: m= (Ev −Es)−(1−Es) FEv
n=Es+(1−Es) FEv
Where:
Es: is the emissivity of the soil.
Ev: the emissivity of the plants.
F: is a factor for internal reflections of the surface whose average value, assuming different geometric distributions, is 0.55 [35]
The calculated average emissivity of an element of the earth's surface was from (NDVI),(with a standard deviation of 0.004), which was obtained. The final expression for LSE is by: [36].

$$E = 0.004 * P_V + 0.986$$

4.6. Land Surface Temperature (LST):

LST is a condition controlled by the energy balance of the surface and atmosphere and the thermal properties of the surface and subsurface media [37]. The Digital Number (DN) values of the thermal bands (bands 10 and 11 in Landsat OLI/TIRS) were converted to absolute irradiance values to retrieve the LST from the raw Landsat datasets, and then the spectral emissivity was adjusted based on the landscape [38]. The pre-processed band 10 from Landsat-8, which includes upper atmosphere brightness temperature values in Kelvin, was applied, converting brightness temperature values to Celsius (C°) to produce an LST map for all study areas. The emissivity-adjusted LST was calculated, Eq.6 [39].

$$LST\ (C^0) = \frac{BT}{1 + (\lambda \times BT/\rho)\ Ln\varepsilon} \quad \text{.....(6)}$$

Where:- - BT: Landsat-8 Band 10 brightness temperature.
- λ: wavelength of emitted radiance (λ=10.8μm, the center wavelength of Landsat-8 Band 10, was applied).
- ρ=h×c/σ (1.438 ×10−2 m K),

where:
- σ = Boltzmann constant (1.38×10^{-23} J/K).
- h=Planck's constant (6.626×10^{-34} Js).
- c = speed of light (2.998×10^{8} m/s).

4.7. Soil Moisture Index (SMI):

Remote sensing and GIS are reliable methods for measuring soil moisture because they can cover a large area quickly. Soil moisture maps are drawn based on land surface temperature [40]. Vegetation indices. This is due to the strong positive correlation between the natural vegetation index and soil surface moisture[41],[42], where vegetation is the parameter that most affects soil moisture. Increased vegetation will deplete soil moisture content (SWC). As for LST, if the surface temperature is low, the surface has low heat transfer, which indicates high soil moisture[43],[44]. SWI was calculated according to the equation

$$SMI = (LST\ \max - LST)/(LSTmax - LSTmin) \quad \text{..... (7)}$$

The final maps of the study area depicting the land surface temperature and soil moisture index were generated after calculating each vegetation cover fraction (Pv), mean brightness temperature(BT), and land surface emissivity(e) along with other standard values such as Boltzmann constant, wavelength of emitted radiation, speed of light, and Planck constant to determine the land surface temperature and soil moisture index.

Results:

1) The Normalized Difference Vegetation Index(NDVI):

It indicates areas where vegetation is present. Landsat image bands 4 and 5 were used to calculate this index. The result shows partly dense vegetation cover in the eastern and northeastern parts of the study area. The vegetation index values ranged between (MAX: 0.554171) and (MIN: -0.291058) in 2013, which is more than what was recorded in 2023, as the values ranged between (MAX: 0.46315) and (MIN: -0.291058), Figure 4.

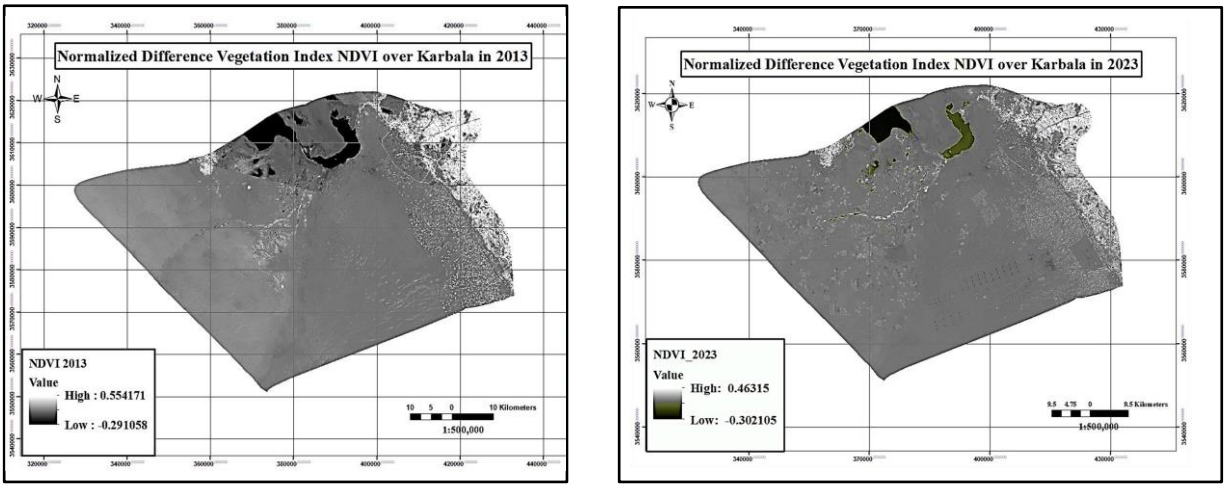

Figure 4: Standardized Vegetation Index map for 2013 and 2023

2) Land Surface Temperature (LST):

The land surface temperature of the study area was determined from satellite data and represents the surface temperatures of each element within a pixel, which may consist of different land cover classes. LST maps of the research area were generated in ten years from 2013 to 2023, using the above equations to analyze data from Landsat-8 Thermal Band 10 in ArcGIS 10.7. This indicates that the surface temperature ranges become higher when comparing the years 2013 and 2023, and high surface temperatures were observed in the city's interior, southern, and western areas due to urban expansion and some exposed areas devoid of vegetation. In contrast, low surface temperatures in the northern areas surrounding the water and vegetation concentration areas in the east and northeast of the study area. Figure 5.

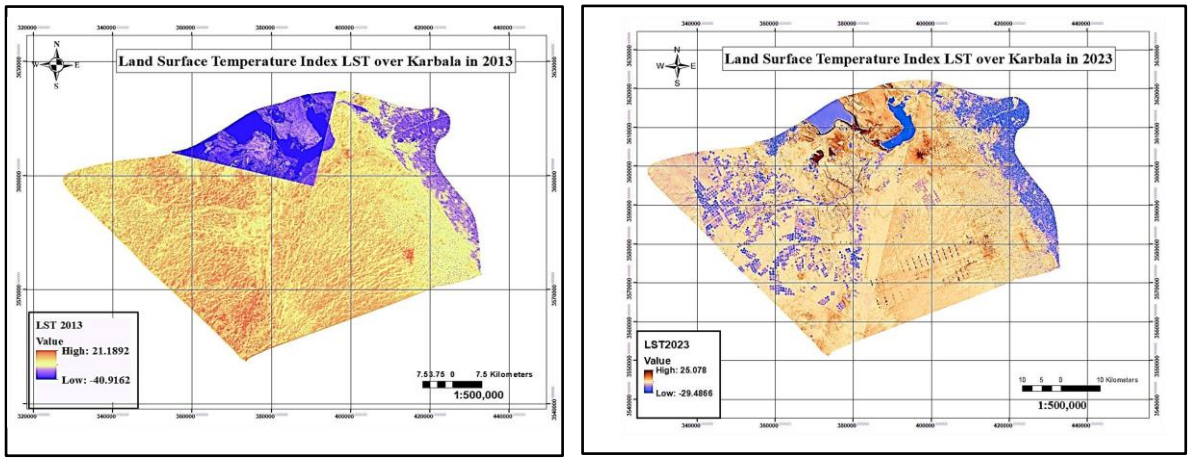

Figure 5: Land surface temperature of Karbala province for 2013 and 2023

3) Soil Moisture Index (SMI):

Figure 6 shows the soil moisture levels for the years 2013 and 2023. SMI maps were created for the research area. It was found that the northern areas have higher soil moisture levels due to their proximity to water bodies and vegetation. In addition, the lowland areas have good moisture conditions. Conversely, other areas in the western part especially have low moisture due to the topography of the surface where the desert lands extend.

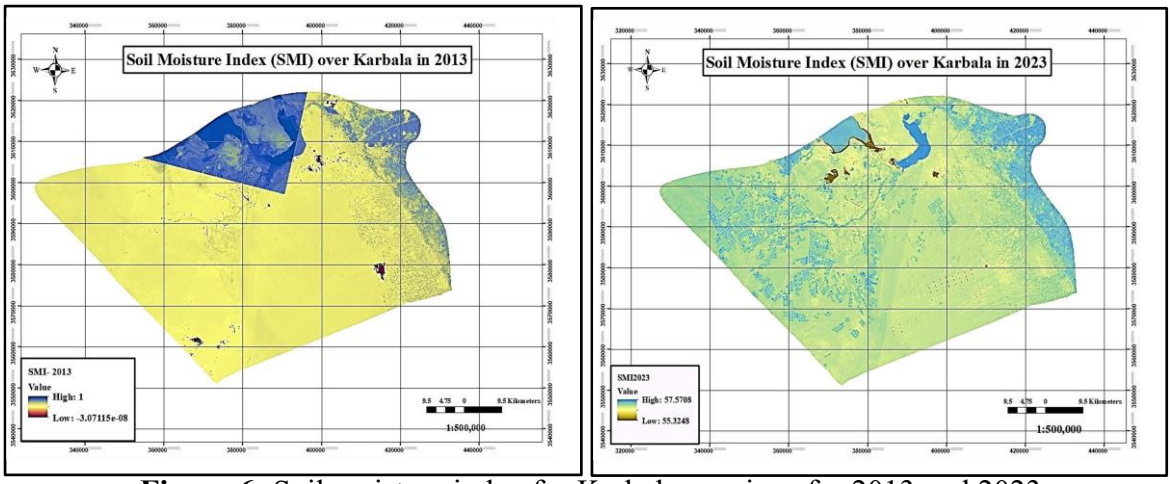

Figure 6: Soil moisture index for Karbala province for 2013 and 2023

This study examined the relationship between vegetation scatterplots (measured by NDVI), LST (surface temperature), and soil moisture (measured by SMI) between 2013 and 2023.

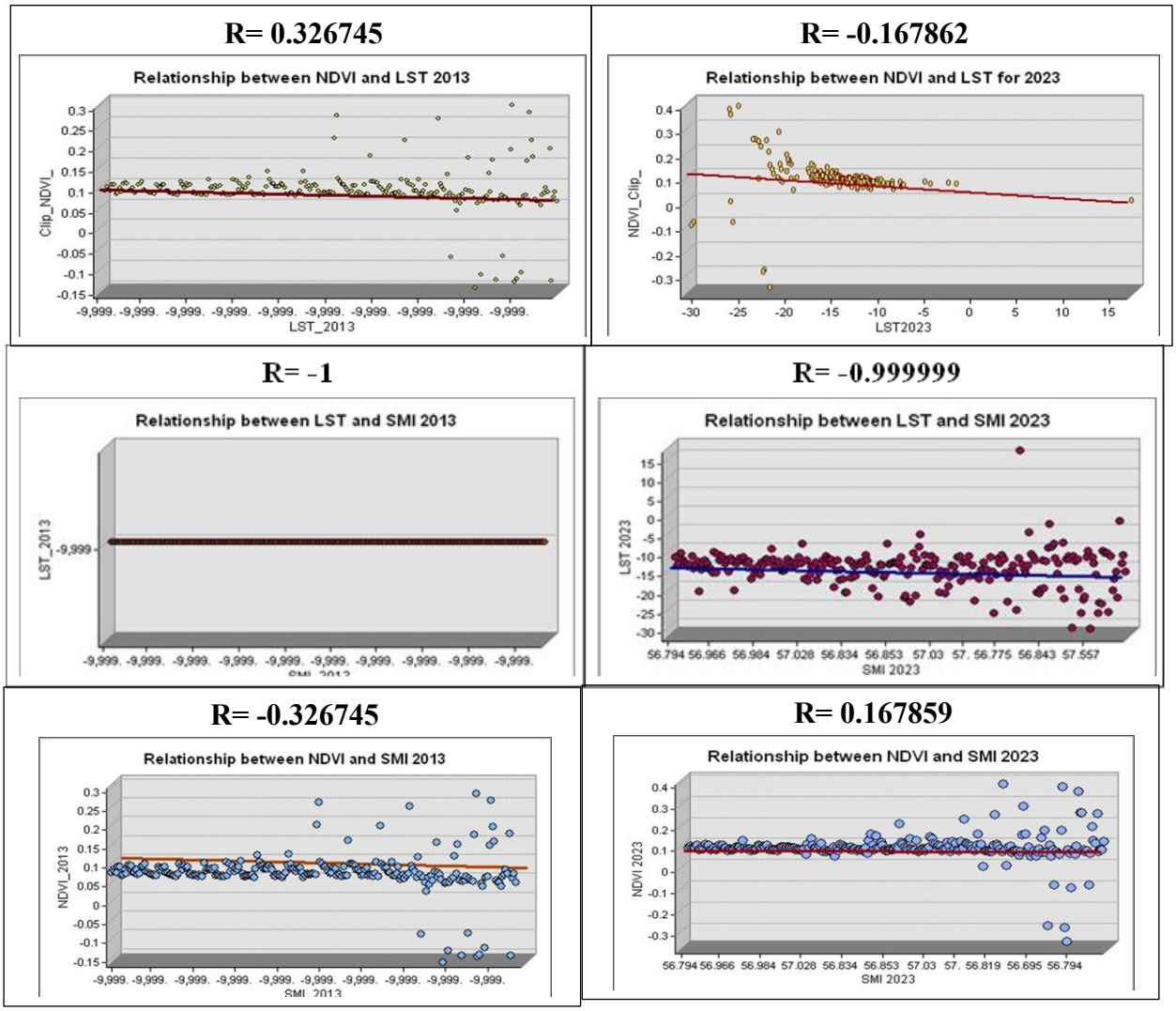

Figure 7: Relationship between NDVI, LST, and SMI using correlation coefficient in 2013 and 2023

Conclusion:

Using remote sensing and GIS techniques, the relationship between (LST) and (SMI) can be estimated, and the variance between these climatic factors can be determined over ten years; the results showed there is a very weak positive correlation between LST and NDVI in 2013, with a correlation coefficient of 0.3, and the relationship weakened over the ten years until it became an inverse relationship in 2023, with a correlation coefficient of -0.16, which means that LST increases with the aridity and density of the environment. Areas with high LST values contrast with those with low NDVI values. A complete inverse correlation exists between LST and SMI in 2013, with a coefficient of -0.1. This relationship continued over ten years until the correlation coefficient reached -0.9 in 2023. There is a weak correlation between the soil moisture index SMI and the Natural Vegetation Index NDVI in 2013. It is clear that the correlation coefficient was around -0.3, and the relationship trended over ten years until it became a direct relationship in 2023, with a correlation coefficient of 0.16. Identifying the two factors facilitates the environmental monitoring process, including the distribution of temperature and humidity conditions in the study area. Their integration enables a drought monitoring system by identifying locations with high temperatures and low soil moisture levels, which can be used in the study area's agriculture, urban planning, or water resources management.

Future studies: Relationship of urban expansion to (LST) &(SMI).

References:

[1] Y. Julien, J. A. Sobrino and W. Verhoef , "Changes in land surface temperatures and NDVI values over Europe between 1982 and 1999," Remote Sensing of Environment, vol. 103, no. 1, pp. 43-55, 15 July 2006.

[2] C. J. Tomlinson, L. Chapman, J. . E. Thornes and C. Baker, "Remote sensing land surface temperature for meteorology : a review," Royal Meteorological Society, p. 296–306, July 2011.

[3] X. Yuan, W. Wang, J. Cui and F. Meng, "Vegetation changes and land surface feedbacks drive shifts in local temperatures over Central Asia," Scientific RepoRt, vol. 7, no. 1, June 2017.

[4] Z –L. Li, S. Duan, "Review of methods for land surface temperature derived from thermal infrared remotely sensed data," Journal of Remote Sensing, vol. 20, no. 5, pp. 899-920, 2016.

[5] W. Zhou, Y.Qian, L. Han, "Relationships between land cover and the surface urban heat island: seasonal variability and effects of spatial and thematic resolution of land cover data on predicting land surface temperatures," Landscape Ecology, vol. 29, no. 1, p. 153–167, 2014.

[6] W. Zhou, J. Wang, and M. Cadenasso, "Effects of the spatial configuration of trees on urban heat mitigation: A comparative study," Remote Sensing of Environment, vol. 195, June 2017.

[7] T. M. Lillesand, R. M. Kiefer and J. W. Chipman, "Remote Sensing and Image Interpretation (Fifth Edition)," Geographical Journal, vol. 146, January 2004.

[8] N. Das, P. Mondal, S. Sutradhar and R. Ghosh, "Assessment of variation of land use/land cover and its impact on land surface temperature of Asansol subdivision," The Egyptian Journal of Remote Sensing and Space Sciences, vol. 24, no. 1, pp. 131-149, February 2021.

[9] I. Dyras, H. Dobesch and E. Grueter, “The use of Geographic Information Systems in climatology and meteorology: COST 719,” Meteorological Applications, vol. 12, no. 1, 2005.

[10] M. Jin, "Analysis of Land Skin Temperature Using AVHRR Observations," Bulletin of the American Meteorological Society, vol. 85, no. 4, April 2004.

[11] Y. K. H. Moussa and A. A. Alwehab, “Evaluation of Climate Change Indicators for Bagdad City Using Remote Sensing Technology,” Iraqi Journal of Science, vol. 64, no. 8, pp. 5190-5201, 2023.

[12] F. K. Mashee, M. . S. J. Al-Zewary, and M. J. Rasheed, "To study climatic factors effect on Land

Covers (LC) for Salah Aldeen region by using remote sensing data," Ecology Environment and Conservation, vol. 26, no. 1, pp. 446-453, 2020.

[13] C. J. Tomlinson, L. Chapman, J. Thornes, and C. J. Baker, "Derivation of Birmingham's summer surface urban heat island from MODIS satellite images," INTERNATIONAL JOURNAL OF CLIMATOLOGY, vol. 32, p. 214 –224, 2012.

[14] M. Imhoff, P. Zhang, R. E. Wolfe, and L. Bounoua, "Remote sensing of the urban heat island effect across biomes in the continental USA," vol. 114, no. 3, pp. 504-513, March 2021.

[15] T. Nitis and N. Moussiopoulos, "The Use of Geoinformatics in Coastal Atmospheric Transport Phenomena: The Athens Experiment," Journal of Marine Science and Engineering, vol. 9, no. 11, October 2021.

[16] Y. Zhang, C. A. Silva, and M. Chen, "Analyzing Thermal EnvironmentContribution and Driving Factors of LstHeterogeneity Based on Urban DifferentDevelopment Zones," Preprints.org (www.preprints.org)/ NOT PEER-REVIEWED, 2024.

[17] Y. Ghobadi, B. Pradhan, H. Shafri and K. Kabiri, "Assessment of spatial relationship between land surface temperature and land use/cover retrieval from multi-temporal remote sensing data in South Karkheh Sub-basin, Iran," vol. 8, no. 1, January 2014.

[18] F. Ferrelli, M. A. H. Cisneros, A. L. Delgado, and M. C. Piccolo, "Spatial and temporal analysis of the LST-NDVI relationship for the study of land cover changes and their contribution to urban planning in Monte Hermoso, Argentina," Documents d'Anàlisi Geogràfica, vol. 64, no. 1, pp. 25-47, 2018.

[19] Y. K. H. Moussa and A. A. Alwehab, "Measuring Changes in Temperature Rates due to Urban Expansion in Selected Municipalities of Baghdad using GIS Technology," Iraqi Journal of Physics, vol. 22, no. 3, pp. 126-138, 2024.

[20] A.E. Frazier, and L. Wang, "Characterizing spatial patterns of invasive species using sub-pixel classifications," Remote Sens. Environ, vol. 115, p. 1997–2007, 2011.

[21] I. J. Muhsin and A. H. Mohammed, "Assessment of vegetal cover changes using Normalized Difference Vegetation Index (NDVI) and subtractive (NDVI) time-series Karbala province, Iraq," Iraqi Journal of Physics, vol. 15, no. 35, 2017.

[22] Y. K. H. Moussa, A. A. Zaeen, H. A. Jasim, M. I. Abdalmajied, E. . H. Khudhair and B. K. Al-Maiyaly, "Measuring Urban Heat Island Indicators from Surface Temperature Using Spatial Techniques," Technologies and Materials for Renewable Energy, Environment and Sustainability, vol. 3028, no. 012051, 2025.

[23] W. Suparta and H. G. Hartono, "Application of the NDBI Method For Determining of Built-Up Land (A Case Study For Surabaya City, Indonesia)," nternational Research Journal of Engineering and Technology (IRJET), vol. 11, no. 7, July 2024.

[24] N. B. Theyab, H. E. Al-Jameel, and R. R. A. Almuhanna, "Impact of Traffic Flow on Pollution at Urban Intersections," Journal of Physics: Conference, vol. 1973, no. 012240, 2021.

[25] A. Shaker, M. . R. Mezaal, M. . R. Hameed and A. Samir, "A Framework for Improving Urban Land Cover Using Object and Pixel-Based Techniques via Remotely Sensed Data," Nature Environment and Pollution Technology, vol. 21, no. 5, December 2022.

[26] USGS Science for a changing world, "USGS EROS registration system · USGS.gov," 2023. [Online].

[27] J. A. Barsi, S. J. Hook, J. R. Schott, and N. G. Raqueno, "Landsat-8 Thermal Infrared Sensor (TIRS) Vicarious," remote sensing, vol. 6, no. 2072-4292, 2014.

[28] Landsat Missions, "Using the USGS Landsat Level-1 Data Product," 2023. [Online].

[29] K. B. Pal, T. B. Chalaune, R. R. Pant, and L. Thapa, "Hydrochemical assessment of the Beeshazar and associated lakes in Central Nepal.," SN Applied Sciences, vol. 3, no. 38, 2021.

[30] U. Avdan and G. Kaplan, "Algorithm for automated mapping of land surface temperature using LANDSAT 8 satellite data," Hindawi Publishing Corporation / Journal of Sensors, vol. 2016, no. 2, 2016.

[31] J. A. Richards, Remote Sensing Digital Image Analysis, SPRINGER, 2022, p. 567.

[32] N. Pettorelli, S. J. Ryan, T. Mueller, and N. Bunnefeld, "The Normalized Difference Vegetation Index (NDVI): unforeseen successes in animal ecology," vol. 46, no. 1, p. 15–27, Jan 2011.

[33] A. S. Al-Turaihi, J. . H. Al-Zubaidi and J. K. Manii, "Vegetation Cover Variations in Central Iraq by Using GIS and Remote Sensing Data," Iraqi Geological Journal, vol. 55, pp. 122-133, 2022.

[34] E. Taktikou, G. Bourazanis, G. Papaioannou, and P., "Prediction of Soil Moisture from Remote Sensing Data," Procedia Eng, vol. 162, pp. 309-316, 2016.

[35] Q. Weijun, C. Hongbi, and H. Xiuzhe, "A Modified Becker's Split-Window Approach for Retrieving Land Surface Temperature from AVHRR and VIRR," ACTA METEOROLOGICA SINICA, vol. 26, no. 2, 2011.

[36] J. Sobrino, J.-C. Jimenez, and L. Paolini, "Land surface temperature retrieval from LANDSAT TM 5," Remote Sensing of Environment, vol. 90, no. 4, 2004.

[37] B. N. K. Naidu and . F. A. Chundeli , "Assessing LULC changes and LST through NDVI and NDBI spatial indicators: a case of Bengaluru, India," GeoJournal, vol. 88, p. 4335–4350, April 2023.

[38] J. A. Sobrino, J. C. J. ´nez-Mun˜oz and L. Paolini, "Land surface temperature retrieval from LANDSAT TM 5," Remote Sensing of Environment, vol. 90, p. 434–440, 2004.

[39] N. Tajudin, N. Ya'acob, D. M. Ali and N. A. Adnan, "Soil moisture index estimation from Landsat 8 images for prediction and monitoring landslide occurrences in Ulu Kelang, Selangor, Malaysia," International Journal of Electrical and Computer Engineering (IJECE), vol. 11, no. 3, 2021.

[40] A. Saha, M. Patil, V. C. Goyal, and D. S. Rathore, "Assessment and Impact of Soil Moisture Index in Agricultural Drought Estimation Using Remote Sensing and GIS Techniques," Proceedings, vol. 7, no. 1, 2018.

[41] N. Arif, T. Sarastika and S. T. Putro, "Land surface temperature (LST) and soil moisture index (SMI) to identify slope stability," IOP Conference Series: Earth and Environmental Science, vol.

[42] 1, 2022.
S. Singh, R. Singh, K. Singh, K. Katoch, A. A. Zaeen, & K. I. Abood ."Smart fertilizer technologies: An environmental impact assessment for sustainable agriculture" , vol.8, 100504, 2024.

[43] M. T. Schnur, H. Xie, and X. Wang, "Estimating root zone soil moisture at distant sites using MODIS NDVI and EVI in a semi-arid region of southwestern USA," Ecological Informatics, vol.

[44] 5, no. 5, 2010.
L. K. Sharma, S. K. Bali, A. A. Zaeen, P. Baldwin, & Franzen, D. W. "Use of rainfall data to improve ground-based active optical sensors yield estimates." Agronomy Journal, 110(4), 1561-1571. 2018